

A Novel Constrained Trajectory Planner for Safe Human-robot Collaboration

Matteo Melchiorre^a, Leonardo Sabatino Scimmi^b, Stefano Mauro^c and Stefano Pastorelli^d
Department of Mechanical and Aerospace Engineering, Politecnico di Torino, C.so Duca degli Abruzzi 24, Turin, Italy

Keywords: Collaborative Robotics, Collision Avoidance, Real-time, Motion Planning.

Abstract: This paper presents a novel collision avoidance algorithm for collaborative robotics that can influence the collision-free trajectory of the robot according to preferred directions with respect to the human posture. The aim is to avoid the human body parts in a controlled manner so that the robot trajectory is predictable. The algorithm is based on closed loop inverse kinematics and uses velocity commands to modify the robot trajectory in real-time. The existing human tracking devices allow to measure the human posture in three dimensions. The idea is to combine the human posture estimation with repulsive volumes, i.e. regions that approximate the human size and that produce repulsive velocities on the robot, and to add attractive surfaces made of cylindrical sectors to condition the avoidance manoeuvre in a chosen direction. The algorithm is tested in a simulation environment built with the model of a collaborative robot and a mock-up of the human, whose motion is generated from real data acquired by 3d vision sensors. The results show the effectiveness of the proposed method during a pick and place task in common scenarios, where the human intersects the robot planned path with different body parts.

1 INTRODUCTION

Human-robot collaboration (HRC) happens when human and robot operate within the same workspace to accomplish a task. The industrial application of HRC is expressed as collaborative robotics. The documents (Krüger, Lien, & Verl, 2009; Vicentini, 2021) give an overview of the most relevant findings and applications. One of the main branches of study concerns the possibility to drive the robot with collision-free trajectories that satisfy task and safety constraints. In particular, responsive collaboration requires the robot to react in real time to human motion, when they both move in the same environment [3].

Adjusting robot trajectory on the go is something that can be dealt with online collision avoidance techniques. Two different approaches can be distinguished. Some studies consider slowing down or stopping the robot when the human is detected in a short range (Byner, Matthias, & Ding, 2019; Corrales, Candelas, & Torres, 2011; Pellegrinelli, Moro,

Pedrocchi, Molinari Tosatti, & Tolio, 2016). However, this reduces task efficiency (Scimmi, Melchiorre, Troise, Mauro, & Pastorelli, 2021). Other works propose to deviate the robot path to achieve a continuous collision-free motion (Chen & Song, 2018; Flacco, Kroger, Luca, & Khatib, 2012; Kaldestad, Haddadin, Belder, Hovland, & Anisi, 2014; Liu & Tomizuka, 2016; Mauro, Scimmi, & Pastorelli, 2017; Melchiorre, Scimmi, Pastorelli, & Mauro, 2019; Merckaert et al., 2022; Parigi Polverini, Zanchettin, & Rocco, 2017; Ragaglia, Zanchettin, & Rocco, 2018; Safeea, Neto, & Bearee, 2019; Schmidt & Wang, 2014; Zanchettin, Rocco, Chiappa, & Rossi, 2019). In the latter, the well-known artificial potential field (APF)-based techniques are the most common (Chen & Song, 2018; Flacco et al., 2012; Kaldestad et al., 2014; Merckaert et al., 2022; Parigi Polverini et al., 2017; Safeea et al., 2019; Schmidt & Wang, 2014). The idea is that the robot navigates attracted by the target, while repulsive effects act nearby the obstacles. Depending on the control law, some algorithms stand on command vector calculated from

^a <https://orcid.org/0000-0002-4409-186X>

^b <https://orcid.org/0000-0002-0537-2984>

^c <https://orcid.org/0000-0001-8395-8297>

^d <https://orcid.org/0000-0001-7808-8776>

the gradient of the potential field, other variants compute repulsive velocity components to be added to the velocity vector related to the target. The main advantages of APF-based techniques are: i) easy implementation; ii) fast computation, as the trajectory is affected locally and does not require to be globally redefined. On the other hand, the drawback of local techniques is that the alternative trajectories are less controllable, since dynamic environments means absent or limited a-priori information on obstacle motion, thus repulsive effect can occur anytime and across any direction during robot motion.

Regarding the execution of the collision-free trajectory, the standards (“ISO/TS 15066. Robots and Robotic Devices: Collaborative Robots,” 2016) do not provide any requirements. However, controlling robot evasive motion according to human preferences can be fundamental. For instance, robot movement predictability affects the psychophysical response of the human (Dragan, Bauman, Forlizzi, & Srinivasa, 2015; Koppenborg, Nickel, Naber, Lungfiel, & Huelke, 2017). The robot motion is predictable if it matches what the human would expect, given the robot task (Dragan et al., 2015). If the robot moves undisturbed, the human can anticipate robot intention due to task repeatability. On the other hand, when the operator is within robot range of motion and collision avoidance activates, the human body represent a dynamic obstacle. In the last case, if the collision avoidance manoeuvre is not controlled in some way, predicting the robot collision-free path can be difficult for the operator.

This work proposes an improved collision avoidance algorithm based on repulsive and attractive velocities that conditions the robot collision-free path in a controlled manner. The originality of the proposed algorithm consists in: i) addressing the alternative path problem in the context of collaborative robotics; ii) combining repulsive and attractive effects around obstacles in a novel form, with a view to evasive and controlled robot motion.

2 HUMAN-ORIENTED COLLISION AVOIDANCE

2.1 Problem Overview

In the context of collision avoidance, representing robot and obstacles real shapes with simple geometries can be convenient for different reasons. In collaborative robotics applications, for example, it is common to approximate the human and robot sizes with cuboids, ellipsoids and cylinders (Byner et al., 2019; Chen & Song, 2018; Corrales et al., 2011; Flacco et al., 2012; Liu & Tomizuka, 2016; Martinez-

Salvador, Perez-Francisco, & Del Pobil, 2003; Merckaert et al., 2022; Parigi Polverini et al., 2017; Pellegrinelli et al., 2016; Safeea et al., 2019). This allows to consider a safety margin varying geometry sizes and simplifies distance calculation.

Concerning collaborative robots, they are usually 6dof manipulators. Reconstructing the pose is straightforward as this can be calculated from feedback signals through direct kinematics. For instance, spheres can be placed along the kinematic chain to enclose the robot body.

As regard the human, due to intrusiveness of wearable sensors, many studies use 3D cameras equipped with human tracking software (Chen & Song, 2018; Flacco et al., 2012; Kaldestad et al., 2014; Melchiorre, Scimmi, Mauro, & Pastorelli, 2021; Parigi Polverini et al., 2017; Pellegrinelli et al., 2016; Ragaglia et al., 2018; Safeea et al., 2019; Schmidt & Wang, 2014; Scimmi et al., 2021; Zanchettin et al., 2019). The output is given in terms of human body joint positions, commonly referred as *skeleton*. This comes in handy when building the human envelope, as geometry elements can be placed on the skeleton.

In Figure 1 an example is shown. A 6dof collaborative robot is represented with n spheres centred in control points, opportunely displaced along the kinematic chain. The human shape is obtained as an augmented skeleton, made of spheres and cylinders. Suppose that the robot task consists in reaching a target position. If the human intersects the planned path, e.g. with his hand as in a collaborative assembly (Scimmi et al., 2021), regardless of the robot path as long as it maintains a protective distance, the task carries on safely. This can be dealt with existing real-time collision avoidance techniques.

However, if the operator can infer a-priori where the robot would pass, the robot motion becomes predictable. For this purpose, the robot trajectory can be constrained, e.g. in front of the hand, so that the human is aware of the alternative path.

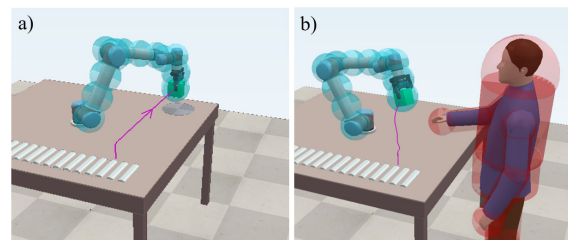


Figure 1: a) Robot planned task. b) Example of Human-robot collision avoidance.

2.2 Attractive and Repulsive Geometries

In the following, with the expression *repulsive geometry* is intended a space region that provides a repulsive effect on the robot. Similarly, the expression *attractive geometry* indicates a region the robot is attracted by.

The role of attractive geometries is to condition the robot path during obstacle avoidance. Consider the example of Figure 1. In combination with the repulsive sphere on the human hand, one can add a cylindrical surface that acts by attracting the robot on a chosen side, as in Figure 2. In this way, the robot would cross the hand on the front side. This is not obvious since by using only the repulsive sphere, the robot can pass either above or below the human hand. With a similar approach, one can use patches attached to any part of the skeleton, e.g., the forearm, to prepare attractive regions at will.

Attractive geometries fixed to the skeleton move according to human motion. Thus, preferred collision avoidance directions are defined relatively to the pose of the body parts. Attractive geometries moving with body parts can be thought for a close collaboration, as the attraction depends on position and orientation of skeleton segments.



Figure 2: Attractive surfaces and repulsive volumes.

2.2.1 Formulation

The formula for repulsive velocities has been introduced in (Flacco et al., 2012). Attractive geometries are introduced in a similar manner, with a formulation that provide a smooth attractive vector field.

As the original usage of attractive regions is one of the main contributions of this work, the related formula is discussed more in depth. After, a summary is also given for repulsive geometries.

Attractive Geometries. In this work, attractive geometries are built from cylindrical primitives.

The role of attractive geometries is to apply an attractive effect in terms of velocity to the end effector of the robot. To orient the attraction, it is convenient using cylindrical sectors, as introduced in Figure 2.

A generic sector of a cylinder is shown in Figure 3. The cylinder is centred in the frame $O_c - x_c y_c z_c$, with the z_c axis aligned with the cylinder axis. The angle θ_a identifies the attractive arc of cylinder. Given θ_a and assuming that the attractive region is symmetric with respect to y_c , the angles θ_s and θ_b are introduced as:

$$\theta_s = \frac{\theta_a}{2}, \quad 0 < \theta_s \leq \pi \quad (1)$$

$$\theta_b = \frac{\pi}{2} - \theta_s, \quad -\frac{\pi}{2} \leq \theta_b < \frac{\pi}{2} \quad (2)$$

Let $\mathbf{p}^c = [p_x^c \ p_y^c \ p_z^c]^T$ denote the generic point C observed in the cylinder frame. The attractive range is limited within the height of the cylinder h_c , so that the attractive velocity acts only for $|p_z^c| \leq h_c/2$. In this case, the intensity of the attraction in \mathbf{p}^c is modelled as a function of the distance from the cylinder. As the distance does not depend on p_z^c , the formula is obtained observing the $x_c y_c$ plane.

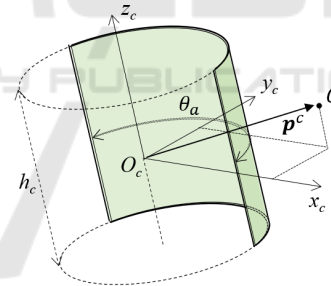


Figure 3: Attractive cylindrical sector.

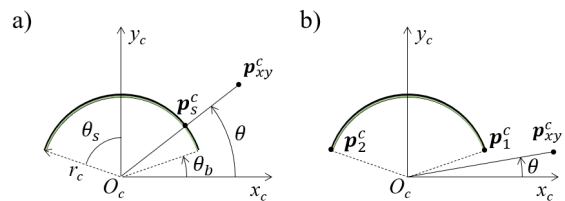


Figure 4: Analysis of the attractive arc.

Let $\mathbf{p}_{xy}^c = [p_x^c \ p_y^c \ 0]^T$ be the projection of the point on the $x_c y_c$ plane. The angle θ is introduced as:

$$\theta = \sin^{-1} \left(\frac{p_y^c}{\|\mathbf{p}_{xy}^c\|} \right), \quad -\frac{\pi}{2} \leq \theta \leq \frac{\pi}{2} \quad (3)$$

The distance d_a from the attractive source depends on θ . Two cases can be distinguished.

$$\text{Case 1: } \theta_b \leq \theta \leq \frac{\pi}{2}$$

The distance is calculated considering the closest point on the surface of the cylinder \mathbf{p}_s^c (see Figure 4a). The displacement \mathbf{d}_a^c is defined as:

$$\mathbf{d}_a^c = \mathbf{p}_s^c - \mathbf{p}_{xy}^c \quad (4)$$

Let r_c be the cylinder radius, \mathbf{p}_s^c can be written as:

$$\mathbf{p}_s^c = \left[r_c \frac{p_x^c}{\|\mathbf{p}_{xy}^c\|} \quad r_c \frac{p_y^c}{\|\mathbf{p}_{xy}^c\|} \quad 0 \right]^T \quad (5)$$

$$\text{Case 2: } -\frac{\pi}{2} \leq \theta < \theta_b$$

Depending on the sign of p_x^c , the distance is computed considering the two ends of the arc, denoted as \mathbf{p}_1^c and \mathbf{p}_2^c (see Figure 4b).

If $p_x^c \geq 0$:

$$\mathbf{d}_a^c = \mathbf{p}_1^c - \mathbf{p}_{xy}^c \quad (6)$$

where \mathbf{p}_1^c can be written as:

$$\mathbf{p}_1^c = [r_c \cos \theta_b \quad r_c \sin \theta_b \quad 0]^T \quad (7)$$

If $p_x^c < 0$:

$$\mathbf{d}_a^c = \mathbf{p}_2^c - \mathbf{p}_{xy}^c \quad (8)$$

with \mathbf{p}_2^c calculated as:

$$\mathbf{p}_2^c = [-r_c \cos \theta_b \quad r_c \sin \theta_b \quad 0]^T \quad (9)$$

The attractive velocity \mathbf{v}_a^c acting at the point \mathbf{p}^c is:

$$\mathbf{v}_a^c = v_a \frac{\mathbf{d}_a^c}{\|\mathbf{d}_a^c\|} \quad (10)$$

where v_a is the magnitude of the attractive velocity, defined as:

$$v_a = \frac{v_{a,max}}{\left(1 + e^{\left(1 - d_a \frac{2}{\rho_a}\right) \alpha_a}\right)} \quad (11)$$

In (11), $v_{a,max}$ indicates the maximum value of the attractive velocity, while α_a and ρ_a are the parameters that regulates the variability of v_a according to $d_a = \|\mathbf{d}_a^c\|$.

An example of an attractive velocity vector field resulting from (10) is shown in Figure 5. A semicylinder is considered, thus $\theta_a = \pi$. The

magnitude v_a has been modelled as in (11), with $v_{a,max} = 0.5 \text{ m/s}$, $\rho_a = 0.2 \text{ m}$ and $\alpha_a = 6$ (see Figure 6a).

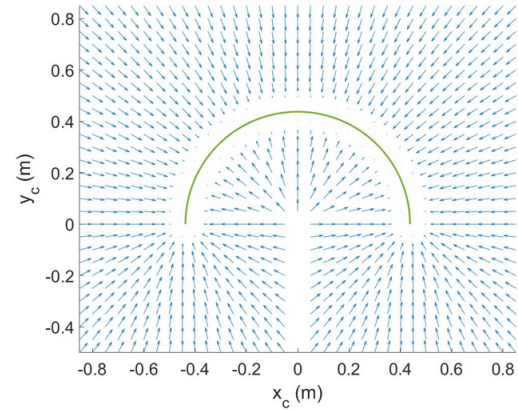


Figure 5: Attractive velocity vector field.

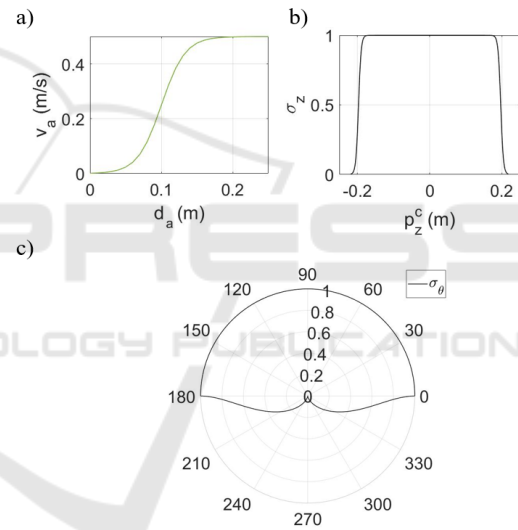


Figure 6: Parameters of the attractive function.

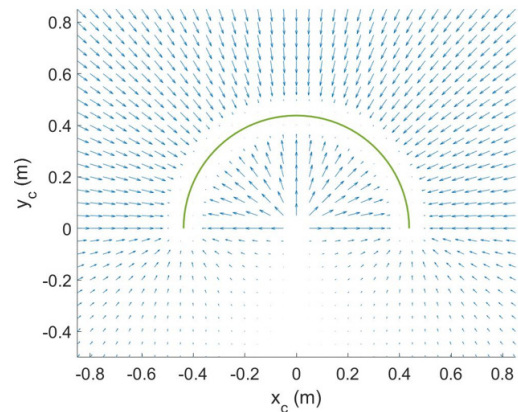


Figure 7: Modified attractive velocity vector field.

By observing Figure 5, the points $p_x^c = 0$ encounter a discontinuity for $p_y^c \leq 0$, i.e. for $\theta = -\frac{\pi}{2}$. Another discontinuity, that is not visible in the two-dimensional representation of Figure 5 but that still exist, is the one at the boundaries when $p_z^c = -h_c/2$ or $p_z^c = h_c/2$.

A smoother transition at the boundaries can be obtained by introducing the coefficients $0 \leq \sigma_z \leq 1$ and $0 \leq \sigma_\theta \leq 1$, so that the attractive velocity in (10) becomes:

$$\mathbf{v}_a^c = \sigma_z \sigma_\theta v_a \frac{\mathbf{d}_a^c}{\|\mathbf{d}_a^c\|} \quad (12)$$

$$\sigma_z = \begin{cases} \frac{1}{\left(1 + e^{\left[1 - \left(\frac{p_z^c + \frac{h_c}{2}}{\rho_z}\right)^2\right] \alpha_z}\right)}, & -\frac{h_c}{2} \leq p_z^c \leq 0 \\ \frac{1}{\left(1 + e^{\left[\left(\frac{p_z^c - \frac{h_c}{2}}{\rho_z}\right)^2 - 1\right] \alpha_z}\right)}, & 0 < p_z^c \leq \frac{h_c}{2} \end{cases} \quad (13)$$

$$\sigma_\theta = \text{real}\left(1 - \sqrt{\sin(\theta + \pi)}\right) \quad (14)$$

In (13), α_z and ρ_z are the parameters that define the shape of σ_z . The functions $\sigma_z(p_z^c)$ and $\sigma_\theta(\theta)$ are plotted in Figure 6b and 6c.

The cardioid function (14) is suited for the application because of the properties of being null for $\theta = -\frac{\pi}{2}$ and of assuming the value 1 for $0 \leq \theta \leq \frac{\pi}{2}$. This is reasonable since the role of the cylindrical sector is to attract the robot on one side of the obstacle. The velocity vector field scaled by the factor σ_θ is represented in Figure 7.

Repulsive Geometries. The human can be seen as a kinematic chain, where the body parts like chest, arms, forearms are connected by joints, such as shoulders and elbows. The size of the body parts which are provided with relative motion can be approximated by capsules, i.e. cylinders rounded with spherical cups at the ends. as in (Liu & Tomizuka, 2016; Safeea et al., 2019). In this work the radius of the cups can also be greater than the cylinder radius. The only constraint is that sphere centers lie on the axis of the cylinder.

The repulsive vector field related to each capsule is computed as a function of the distance from the geometry. The difference with attractive cylindrical sectors is that repulsive regions are intended as volumes that robot cannot access. Thus, repulsive vector fields are defined only outside of this region. On the other hand, the attractive geometry can be seen as an attractive wall, that can be an open surface.

To calculate the distance between a generic point and a capsule, it is convenient observing the point in

the frame $O_c - x_c y_c z_c$, with z_c aligned with the axis of the cylinder and O_c placed at the middle. Let \mathbf{p}_{s1}^c and \mathbf{p}_{s2}^c denote the centers of the spheres of radii r_{s1} and r_{s2} respectively, the displacements between \mathbf{p}^c and its projections on the spherical cups are:

$$\mathbf{d}_{r1}^c = (\mathbf{p}^c - \mathbf{p}_{s1}^c) - r_{s1} \frac{\mathbf{p}^c - \mathbf{p}_{s1}^c}{\|\mathbf{p}^c - \mathbf{p}_{s1}^c\|} \quad (15)$$

$$\mathbf{d}_{r2}^c = (\mathbf{p}^c - \mathbf{p}_{s2}^c) - r_{s2} \frac{\mathbf{p}^c - \mathbf{p}_{s2}^c}{\|\mathbf{p}^c - \mathbf{p}_{s2}^c\|} \quad (16)$$

For the lateral surface of the cylinder, the displacement is defined like (4), but with opposite direction:

$$\mathbf{d}_{r3}^c = \mathbf{p}_{xy}^c - \mathbf{p}_s^c \quad (17)$$

The repulsive distance d_r from the capsule is obtained as:

$$d_r = \begin{cases} \min(d_{r1}, d_{r2}, d_{r3}) & , |p_z^c| \leq h_c/2 \\ \min(d_{r1}, d_{r2}) & , p_z^c > h_c/2 \\ \min(d_{r1}, d_{r2}) & , p_z^c < h_c/2 \end{cases} \quad (18)$$

Thus, the repulsive velocity \mathbf{v}_r acting at the point \mathbf{p} is obtained as:

$$\mathbf{v}_r^c = v_r \frac{\mathbf{d}_r^c}{\|\mathbf{d}_r^c\|} \quad (19)$$

where \mathbf{d}_r^c is (15), (16) or (17), depending on the minimum value resulting from (18). The magnitude of the repulsive velocity v_r , defined as:

$$v_r = \frac{v_{r,max}}{\left(1 + e^{\left(\frac{d_r}{\rho_r} - 1\right) \alpha_r}\right)} \quad (20)$$

In (18), the parameters $v_{r,max}$, α_r and ρ_r have the same meaning of the ones introduced in (11).

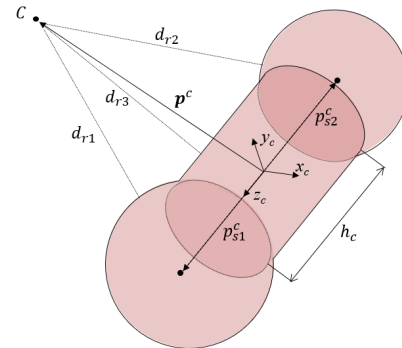


Figure 8: Point-capsule distance calculation.

2.3 Collision Avoidance Strategy

As introduced in Section 2.2, the idea is that the robot navigates in a vector field which is the sum of repulsive and attractive sources opportunely placed on the human shape.

The repulsive action can be dealt with the multiple collision avoidance algorithm presented in (Scimmi, Melchiorre, Mauro, & Pastorelli, 2018) that consider repulsive velocities on each link of the robot depending on human-robot distances.

To simplify distance calculation, the size of the generic link l_i of the robot is approximated with a number n_i of spheres centred in $\mathbf{p}_{i,j}$, with $j = 1, 2 \dots n_i$, as shown in Figure 9. With a similar approach, human body parts can be represented by capsules.

For each point $\mathbf{p}_{i,j}$, the distance from each repulsive source can be evaluated with (18). Let $d_{r,j}$ be the distance between the control point $\mathbf{p}_{i,j}$ and the closest repulsive source. Thus, the minimum distance between the robot link and the human is obtained as:

$$d_{r,i} = \min(d_{r,1}, d_{r,2}, \dots, d_{r,n_i}) - r_i \quad (21)$$

where r_i is the radius of the sphere of the robot link. The repulsive velocity (19) is applied to the control point related to $d_{r,j}$ (e.g. point $\mathbf{p}_{i,4}$ in Figure 9).

Commands to the robot are given in terms of joint velocities $\dot{\mathbf{q}}_i$:

$$\dot{\mathbf{q}}_i = \mathbf{J}_{p,i}^T(\mathbf{q}_i) \mathbf{v}_{r,i} \quad (22)$$

where $\mathbf{v}_{r,i}$ is the repulsive velocity related to l_i , \mathbf{q}_i is the vector of joint positions that affect the motion of l_i and $\mathbf{J}_{p,i}$ is the partial Jacobian related to the control point the repulsive action is applied on. Notice that $\mathbf{J}_{p,i}$ is a three-row matrix that affects the end-effector linear velocity only (Siciliano, Sciavicco, Villani, & Oriolo, 2009).

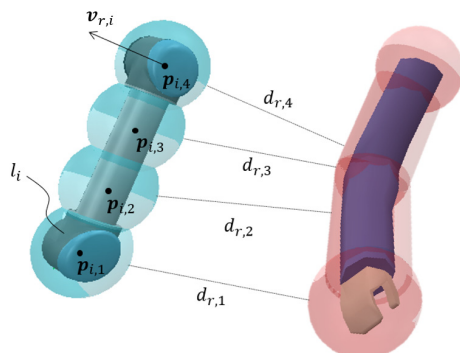


Figure 9: Robot link-capsule distances.

Concerning the attraction, it is limited to the end-effector. To describe how to combine attraction with repulsion, the example of the human hand is considered. However, the same strategy can be applied for any repulsive source.

Assume that one wants to influence the robot end-effector \mathbf{p}_e so that it chooses passing in front of the hand during collision avoidance. An attractive source as in Figure 3 can be centred on the hand. The direction of the attractive cylinder y_c axis is identified considering the segment connecting the elbow to the hand. Besides, the z_c axis of the attractive cylinder is chosen perpendicular to the plane defined by hand, elbow and shoulder.

Let r_e be the radius of the robot sphere centred in the control point \mathbf{p}_e . The strategy consists of activating both attraction and repulsion effects after that \mathbf{p}_e crosses the attractive surface. A possible solution is to set $\mathbf{v}_a = 0$ outside of r_c and to choose the radius and the height of the attractive cylinder as:

$$r_c = r_h + r_e + \rho_r \quad (23)$$

$$h_c = 2r_c \quad (24)$$

where r_h identifies the radius of the spherical cup on the hand side.

The strategy is illustrated in Figure 10. For clarity, only the capsule of the forearm is represented. Outside of the attractive cylinder the end-effector moves undisturbed, according to the planned velocity \mathbf{v}_t . Inside the attractive cylinder, attraction and repulsive velocities are added up for path conditioning.

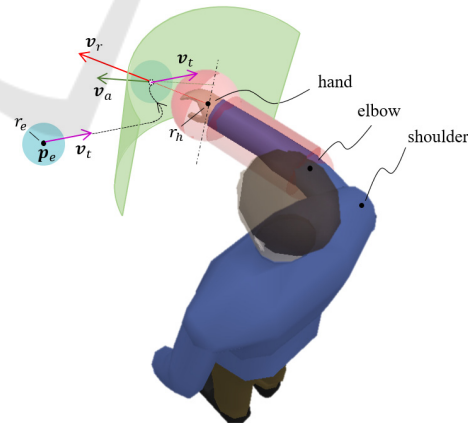


Figure 10: Example of collision avoidance strategy applied to the human hand.

In terms of robot commands, formula (22) is extended to also consider the contribution of \mathbf{v}_t and \mathbf{v}_a . Let the generic pose of the end-effector be denoted as $\mathbf{x}_e = [\mathbf{p}_e \ \boldsymbol{\phi}_e]^T$, where $\boldsymbol{\phi}_e$ is the (3×1) vector that defines the orientation. Assume the

trajectory related to the task has been planned as $\dot{\mathbf{x}}_t = [\mathbf{v}_t \ \boldsymbol{\omega}_t]^T$. The attractive term $\dot{\mathbf{x}}_a = [\mathbf{v}_a \ \mathbf{0}]^T$ and the repulsive term (22) are considered in the inverse kinematic algorithm based on inverted Jacobian (Siciliano et al., 2009):

$$\dot{\mathbf{q}} = J^{-1}(\mathbf{q})(\dot{\mathbf{x}}_t + K\mathbf{e} + \dot{\mathbf{x}}_a) + \sum_i \dot{\mathbf{q}}_i \quad (25)$$

where $\dot{\mathbf{q}}$ is the vector of joint velocities, $J(\mathbf{q})$ is the Jacobian of the end-effector, K is the control gain related to the error $\mathbf{e} = \mathbf{x}_t - \mathbf{x}_e$ between the planned and the actual end-effector poses.

3 APPLICATION

The presented method is applied to collaborative robotics in a significant scenario, where the operator accesses the robot workspace during a pick and place. This can be a subtask of collaborative assembly in which the human is employed for added value operations and the robot collects the parts to be assembled (Scimmi et al., 2021).

The effectiveness of attractive geometries displaced on the human hand rather than on the forearm is investigated considering two different movements of the human. In the following sections, the simulation environment is described and test results are discussed.

3.1 Simulation Tools

The task is simulated in Matlab and visualized in CoppeliaSim. Robot commands and human movements are processed in Matlab. During the simulation, robot and human joint positions are sent to CoppeliaSim for visualization.

A kinematic model of the collaborative robot UR5 is implemented in Matlab, according to joint position and velocity ranges specified in (Universal Robots, n.d., 2022). The robot is approximated with 12 control spheres, divided into $i = 5$ groups, each of them identifying a link after the base along the kinematic chain (see Figure 11). The human is modelled with rigid bodies connected by spherical and revolute joints, as shown in Figure 11. Each body is enclosed by a capsule. In a real-world application, where human motion can be tracked as a skeleton, this would allow for safety margins to be considered and for easy distance calculation.

To consider human-like motion, the human mock-up in the simulation environment moves according to real data acquired by Kinect v2 sensor with a sampling rate of 30 Hz. In particular, real human motion is previously acquired as skeleton points positions in Matlab; thus, joints rotations are

evaluated through inverse kinematics of the human model and sent to CoppeliaSim.

The simulation script consists of a loop running at 30 Hz. For each simulation step, human and robot distances are computed, and robot motion is obtained from first order integration of the control law (25).

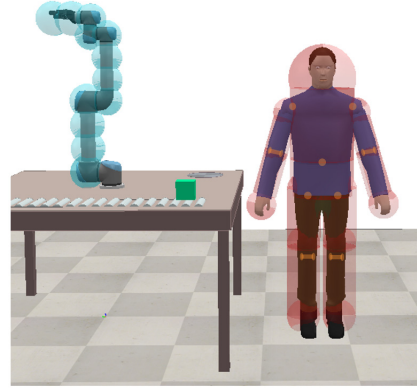


Figure 11: Robot and Human model in CoppeliaSim.

3.2 Results

The algorithm is tested in a pick and place task. The task consists of two phases.

In the first phase, the robot starts from the home position, it picks an object on the workbench with an upward vertical path and then it is expected to follow a horizontal path as in Figure 1a until place position. In the second phase, the robot releases the object with a downward vertical motion, then it is expected to go back to the home position along a retracing horizontal path.

Two tests are proposed, with the operator accessing the robot sub-workspaces where the horizontal displacements are planned. The aim is to bend the robot path on the side of the attractive arcs, as presented in section 2.2.

In Test 1, the human intercepts the planned path of the robot with his right hand during the first phase. To drive the end-effector in front of the hand, an attractive cylinder is applied as described in Figure 10. The attractive effect only activates when the human is within the robot workspace. Results are shown in Figure 12, Test 1a. In particular, the test is carried out considering $r_h = 0.0875 \text{ m}$, $r_e = 0.1 \text{ m}$, $r_c = 0.4375 \text{ m}$, parameters of the attractive velocity as presented in section 2.2.1 (except for $\theta_a = 2\pi/3$), and parameters of the repulsive effect set to $v_{r,max} = 1 \text{ m/s}$, $\rho_r = 0.25 \text{ m}$, $\alpha_r = 6$.

The collision avoidance path is analysed in Figure 13, with all the elements in the scene. Notice that, as the human moves during the robot task, the pose depicted for attractive and repulsive geometries are only representative of a relevant frame. The presence

of the attractive cylinder influences the end-effector passing on the side identified by the direction of the y_c axis (green arrow). In comparison, the classical approach with only repulsive velocities, identified as Test 1b in Figure 12, produces an alternative path above the human hand, as shown in Figure 14.

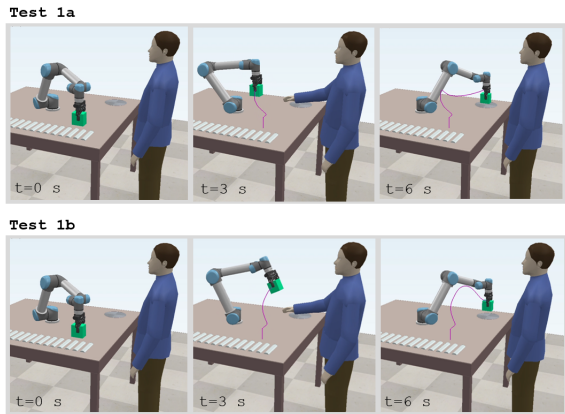


Figure 12: Frames of Test 1.

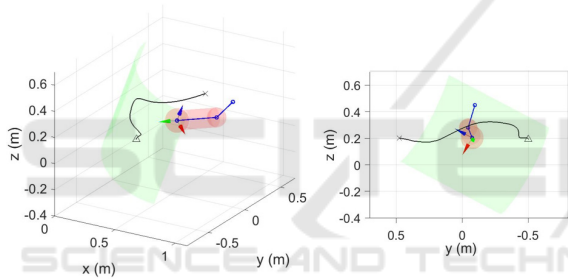


Figure 13: Alternative path of the end-effector in Test 1a.

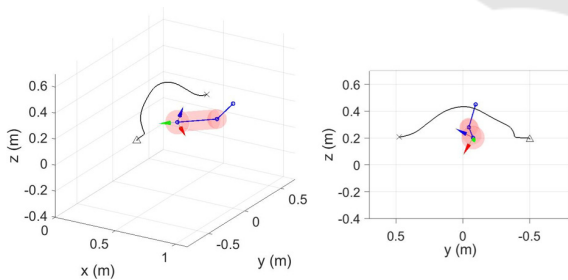


Figure 14: Alternative path of the end-effector in Test 1b.

In Test 2, the human intercepts the robot planned path with the forearm during the second phase of the robot task. An attractive arc with $\theta_a = 2\pi/9$ is placed on the forearm, so that z_c is aligned with the line connecting the elbow to the hand and y_c is perpendicular to the plane defined by hand, elbow and shoulder. The reason behind a narrow θ_a lies on the coupling with the repulsive cylinder. In fact, due to the same geometric primitives, the case $\theta_b \leq \theta \leq \frac{\pi}{2}$

produces an attractive component that has the same direction of the repulsive one. However, the use of a small θ_a moves the attraction towards the ends of the arc, as defined for $-\frac{\pi}{2} \leq \theta < \theta_b$. This effect forces the robot to pass above the forearm, as shown in Figure 15, Test 2a. The related end-effector path is illustrated in Figure 16.

In comparison, the case with only repulsive velocities is not able to produce an alternative path. This is shown in Figure 15, Test 2b. The robot crosses the forearm, but the repulsive direction does not drive the end-effector upward. Moreover, the human movement is more intrusive compared to Test 1 and the robot gets trapped. The robot stops when the minimum distance with the human envelope is less than a safety margin equal to 0.05 m . This can be seen in Figure 17, where the human-robot minimum distance and the end-effector velocity are plotted. When the operator retracts the arm, the minimum distance rises over the safety margin and the robot continues its motion towards the home position.

Moreover, Test 2 shows the capability of the attractive arc to drive the robot towards a preferred direction, pointing out also a limitation of the classical approach.

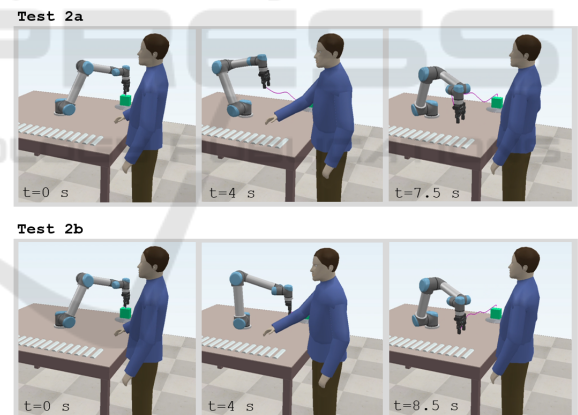


Figure 15: Frames of Test 2.

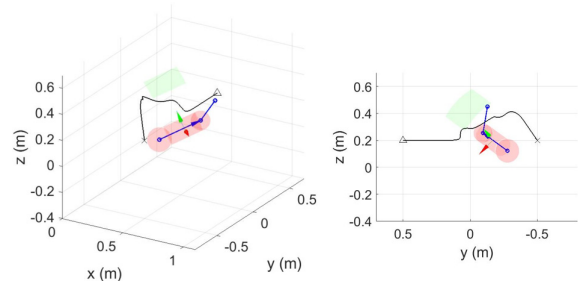


Figure 16: Alternative path of the end-effector in Test 2a.

In fact, by observing the curves in Figure 17, it is evident the increased efficiency in terms of task time, as in Test 2a the robot reaches the home position 1 s before Test 2b. Notice that in each test the magnitude of the end-effector velocity has been limited to 0.25 m/s due to safety concerns.

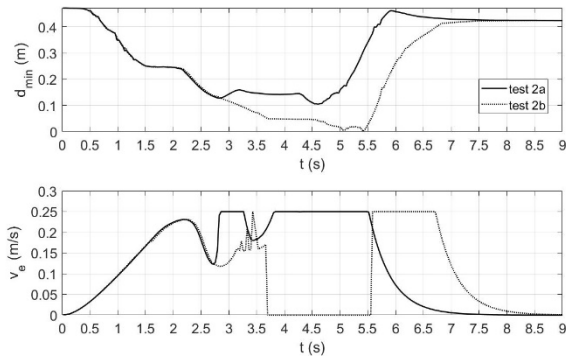


Figure 17: Comparison of minimum distance and end-effector velocity of Test 2a and Test 2b.

4 CONCLUSIONS

The state of the art on human robot collaboration suggested that there is a lack of contributions on conditioning collision-free robot trajectories according to human preferences. In this work, an effective solution based on attractive and repulsive geometries opportunely placed around the human has been proposed. The combination of repulsive volume with attractive effects is novel. The attraction has been related to cylindrical sectors, whose features can be modified at will to fit the body part and to produce attractive velocity components along preferred directions.

To evaluate the effectiveness of the algorithm, a simulation environment made of a collaborative robot UR5 and a human dummy has been used. To simulate human-like motion, the dummy is moved according to data previously acquired by two Kinect sensors in duplex configuration. A pick and place task has been considered, as this can be a subtask of a collaborative assembly. Results have shown that by placing attractive cylindrical sectors on the hand rather than on the forearm of the operator, the collision avoidance path can be influenced in some way. The robot is forced passing in front of the hand or above the forearm during the avoidance manoeuvre. This allows to choose a priori the collision avoidance direction.

Future works will regard the possibility to use different attractive geometries, e.g. spherical sectors and planes, and the experimental application in a real world scenario to evaluate the robustness of the proposed approach in different operating conditions.

REFERENCES

- Byner, C., Matthias, B., & Ding, H. (2019). Dynamic speed and separation monitoring for collaborative robot applications – Concepts and performance. *Robotics and Computer-Integrated Manufacturing*, 58(September 2018), 239–252. <https://doi.org/10.1016/j.rcim.2018.11.002>
- Chen, J.-H., & Song, K.-T. (2018). Collision-Free Motion Planning for Human-Robot Collaborative Safety Under Cartesian Constraint. *2018 IEEE International Conference on Robotics and Automation (ICRA)*, 1–7. <https://doi.org/10.1109/ICRA.2018.8460185>
- Corrales, J. A., Candelas, F. A., & Torres, F. (2011). Safe human – robot interaction based on dynamic sphere-swept line bounding volumes. *Robotics and Computer-Integrated Manufacturing*, 27, 177–185. <https://doi.org/10.1016/j.rcim.2010.07.005>
- Dragan, A. D., Bauman, S., Forlizzi, J., & Srinivasa, S. S. (2015). Effects of Robot Motion on Human-Robot Collaboration. In *ACM/IEEE International Conference on Human-Robot Interaction* (pp. 51–58). ACM. <https://doi.org/10.1145/2696454.2696473>
- Flacco, F., Kroger, T., Luca, A. De, & Khatib, O. (2012). A Depth Space Approach to Human-Robot Collision Avoidance. *IEEE International Conference on Robotics and Automation*.
- ISO/TS 15066. Robots and Robotic Devices: Collaborative Robots. (2016). *International Organization for Standardization*. Geneva, Switzerland.
- Kaldestad, K. B., Haddadin, S., Belder, R., Hovland, G., & Anisi, D. A. (2014). Collision avoidance with potential fields based on parallel processing of 3D-point cloud data on the GPU. *Proceedings - IEEE International Conference on Robotics and Automation*, 3250–3257. <https://doi.org/10.1109/ICRA.2014.6907326>
- Koppenborg, M., Nickel, P., Naber, B., Lungfiel, A., & Huelke, M. (2017). Effects of movement speed and predictability in human – robot collaboration. *Human Factors and Ergonomics in Manufacturing & Service Industries*, 27(4), 197–209. <https://doi.org/10.1002/hfm.20703>
- Krüger, J., Lien, T. K., & Verl, A. (2009). Cooperation of human and machines in assembly lines. *CIRP Annals - Manufacturing Technology*, 58(2), 628–646. <https://doi.org/10.1016/j.cirp.2009.09.009>
- Liu, C., & Tomizuka, M. (2016). Algorithmic Safety Measures for Intelligent Industrial Co-Robots. *2016 IEEE International Conference on Robotics and Automation (ICRA)*, 3095–3102. <https://doi.org/10.1109/ICRA.2016.7487476>
- Martinez-Salvador, B., Perez-Francisco, M., & Del Pobil, A. P. (2003). Collision detection between robot arms and people. *Journal Of Intelligent and Robotic Systems*, 38, 105–119. <https://doi.org/10.1023/A>
- Mauro, S., Scimmi, L. S., & Pastorelli, S. (2017). Collision avoidance algorithm for collaborative robotics. *International Journal of Automation Technology*, 11(3), 481–489. https://doi.org/10.1007/978-3-319-61276-8_38

- Melchiorre, M., Scimmi, L. S., Mauro, S., & Pastorelli, S. P. (2021). Vision-based control architecture for human–robot hand-over applications. *Asian Journal of Control*, 23(1), 105–117. <https://doi.org/10.1002/asjc.2480>
- Melchiorre, M., Scimmi, L. S., Pastorelli, S. P., & Mauro, S. (2019). Collision Avoidance using Point Cloud Data Fusion from Multiple Depth Sensors: A Practical Approach. *2019 23rd International Conference on Mechatronics Technology, ICMT 2019*. <https://doi.org/10.1109/ICMECT.2019.8932143>
- Merckaert, K., Convens, B., Wu, C. ju, Roncone, A., Nicotra, M. M., & Vanderborght, B. (2022). Real-time motion control of robotic manipulators for safe human–robot coexistence. *Robotics and Computer-Integrated Manufacturing*, 73(July 2021), 102223. <https://doi.org/10.1016/j.rcim.2021.102223>
- Parigi Polverini, M., Zanchettin, A. M., & Rocco, P. (2017). A computationally efficient safety assessment for collaborative robotics applications. *Robotics and Computer-Integrated Manufacturing*, 46(November 2016), 25–37. <https://doi.org/10.1016/j.rcim.2016.11.002>
- Pellegrinelli, S., Moro, F. L., Pedrocchi, N., Molinari Tosatti, L., & Tolio, T. (2016). A probabilistic approach to workspace sharing for human–robot cooperation in assembly tasks. *CIRP Annals - Manufacturing Technology*, 65(1), 57–60. <https://doi.org/10.1016/j.cirp.2016.04.035>
- Ragaglia, M., Zanchettin, A. M., & Rocco, P. (2018). Trajectory generation algorithm for safe human-robot collaboration based on multiple depth sensor measurements. *Mechatronics*, 55(December 2017), 267–281. <https://doi.org/10.1016/j.mechatronics.2017.12.009>
- Safeea, M., Neto, P., & Bearee, R. (2019). On-line collision avoidance for collaborative robot manipulators by adjusting off-line generated paths: An industrial use case. *Robotics and Autonomous Systems*, 119, 278–288. <https://doi.org/10.1016/j.robot.2019.07.013>
- Schmidt, B., & Wang, L. (2014). Depth camera based collision avoidance via active robot control. *Journal of Manufacturing Systems*, 33(4), 711–718. <https://doi.org/10.1016/j.jmsy.2014.04.004>
- Scimmi, L. S., Melchiorre, M., Mauro, S., & Pastorelli, S. (2018). Multiple collision avoidance between human limbs and robot links algorithm in collaborative tasks. *ICINCO 2018 - Proceedings of the 15th International Conference on Informatics in Control, Automation and Robotics*, 2, 291–298. <https://doi.org/10.5220/0006852202910298>
- Scimmi, L. S., Melchiorre, M., Troise, M., Mauro, S., & Pastorelli, S. (2021). A Practical and Effective Layout for a Safe Human-Robot Collaborative Assembly Task. *Applied Sciences (Switzerland)*, 11(4).
- Siciliano, B., Sciavicco, L., Villani, L., & Oriolo, G. (2009). *Robotics - Modelling, Planning and Control*. *Journal of Chemical Information and Modeling*.
- Universal Robots. (n.d.). UR5 CB-Series Technical details. Retrieved May 4, 2022, from <https://www.universal-robots.com/download-center/#/cb-series/ur5>
- Universal Robots. (2022). DH parameters for calculations of kinematics and dynamics. Retrieved May 4, 2022, from <https://www.universal-robots.com/articles/ur/application-installation/dh-parameters-for-calculations-of-kinematics-and-dynamics/>
- Vicentini, F. (2021). Collaborative Robotics: A Survey. *Journal of Mechanical Design, Transactions of the ASME*, 143(4), 1–20. <https://doi.org/10.1115/1.4046238>
- Zanchettin, A. M., Rocco, P., Chiappa, S., & Rossi, R. (2019). Towards an optimal avoidance strategy for collaborative robots. *Robotics and Computer-Integrated Manufacturing*, 59(June 2018), 47–55. <https://doi.org/10.1016/j.rcim.2019.01.015>